Stress Domains in Si(111)/a-Si_3N_4 Nanopixel: Ten-Million-Atom Molecular Dynamics Simulations on Parallel Computers

Andrey Omeltchenko, Martina E. Bachlechner, Aiichiro Nakano, Rajiv K. Kalia, and Priya Vashishta
Concurrent Computing Laboratory for Materials Simulations, Department of Physics & Astronomy, and Department of Computer Science, Louisiana State University, Baton Rouge, Louisiana 70803-4001

Ingvar Ebbsjö
Studsvik Neutron Research Laboratory, University of Uppsala, S-611 82 Nyköping, Sweden

Anupam Madhukar
Department of Materials Science and Engineering, University of Southern California, Los Angeles, California 90089-0241

Paul Messina
Center for Advanced Computing Research, California Institute of Technology, Pasadena, California 91125
(Received 17 February 1998; revised manuscript received 14 July 1999)

Parallel molecular dynamics simulations are performed to determine atomic-level stresses in Si(111)/Si_3N_4(0001) and Si(111)/a-Si_3N_4 nanopixels. Compared to the crystalline case, the stresses in amorphous Si_3N_4 are highly inhomogeneous in the plane of the interface. In silicon below the interface, for a 25 nm square mesa stress domains with triangular symmetry are observed, whereas for a rectangular, 54 nm $\times$ 33 nm, mesa tensile stress domains ($\sim$300 Å) are separated by Y-shaped compressive domain wall. Maximum stresses in the domains and domain walls are -2 GPa and $+2$ GPa, respectively.

PACS numbers: 68.35.–p, 02.70.Ns, 61.43.Er, 79.60.Jv

Silicon nitride deposited on a Si substrate is one of the major materials for dielectric layers in microelectronics. With pixel sizes steadily approaching nanometer length scales, there is a growing need to achieve better control over the deposition and etching processes. An important part of this task is the development of reliable physical models for Si/Si_3N_4 interfaces, which can supplement empirical data in nanopixel design and intelligent process control.

Reliable atomistic description of Si_3N_4 and Si/Si_3N_4 interface is provided by the *ab initio* electronic structure approach [1–3]. However, many interesting phenomena are associated with length scales far beyond those accessible to electronic structure calculations. It is therefore important to transfer the atomistic description into a form suitable for large-scale molecular dynamics (MD) [4,5] and thus extend the range of length scales accessible to atomistic modeling.

One of the issues large-scale MD simulations can address is the atomic-level stress distribution in a nanopixel. The stresses induced by surfaces, edges, and interfaces are the major sources of defects and inhomogeneities in the system [6,7] and become increasingly significant for pixel sizes in the nanometer range. Atomistic simulations of stresses in nanostructures may be used as a tool to develop and validate continuum models [8,9].

In this Letter, we report the results of multimillion atom MD simulations of Si/Si/Si_3N_4 nanopixels. We studied both crystalline and amorphous silicon nitride placed on Si(111) nanopixels with the geometries shown in Figs. 1(a) and 2(a). Our systems contain 3.7×10^6 to 10×10^6 atoms resulting in nanopixel sizes not far below that achievable in semiconductor engineering. By using MD simulation, we hope to capture molecular-scale mechanisms affecting the stress state of the system which are not described in a continuum elasticity approach.

Interatomic potentials for Si and Si_3N_4 are used in combination with the charge transfer computed by self-consistent localized atomic orbital (LCAO) electronic structure calculations [3] to construct a realistic Si(111)/Si_3N_4(0001) interface model [10] suitable for large-scale MD simulations. In our model, we have to distinguish between Si atoms in the silicon crystal and in silicon nitride. In addition, the atoms at or near the interface have to be treated differently due to different charge transfer when compared to their bulk counterparts. For bulk Si, we have chosen the Stillinger-Weber [11] potential. The potential for bulk silicon nitride is constructed from two-body (charge transfer, electronic polarizability, and steric repulsion) and three-body (bond bending and stretching) terms [12]. This interatomic potential has been validated by comparison with experimental properties of crystalline and amorphous Si_3N_4 [12,13]. For atoms at the interface, the charge transfer, bond lengths, and bond angles are consistent with chemical bonding considerations and the results of the electronic structure calculations [1,3,10].

Si_3N_4 films deposited on the Si(111) surface are usually amorphous [14], but a coherent Si(111)/Si_3N_4(0001) interface has also been experimentally observed [15]: A unit cell of Si_3N_4 almost perfectly matches 2×2 periodic cells of the Si(111) surface with only a small lattice mismatch. [The Si(111) is 1.1% smaller.] In our

 0031-9007/00/84(2)/318(4)$15.00

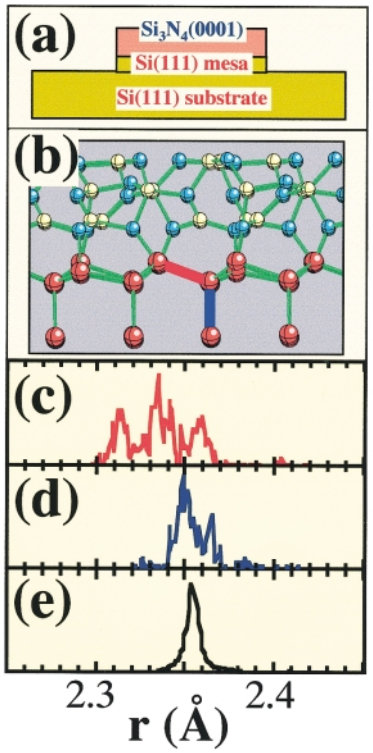

FIG. 1 (color). (a) Schematic of a nanopixel with *crystalline* Si_3N_4. (b) Ball-and-stick figure showing atoms near the interface: Si (yellow) and N (cyan) in Si_3N_4, and Si (red) atoms in silicon. Si-Si bond-length distribution in silicon mesa: (c) bonds between first (top) and second layers of Si atoms, (d) bonds between second and third layer atoms, and (e) bonds in the bulk silicon.

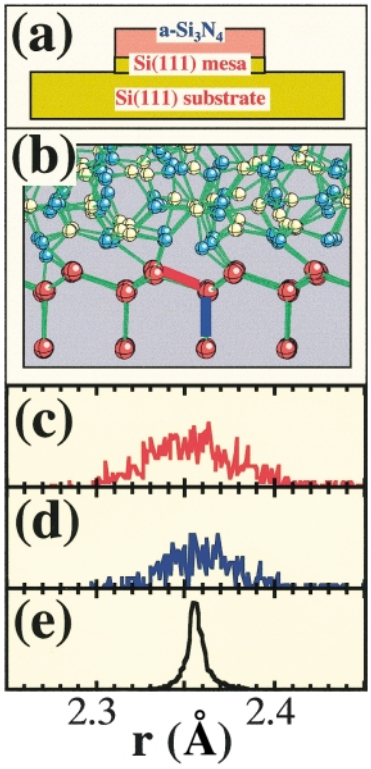

FIG. 2 (color). (a) Schematic of a nanopixel with *amorphous* Si_3N_4. (b)–(e) Same as Fig. 1.

simulations the Si and Si_3N_4 parts of the systems are placed at a distance of 6 Å and then gradually brought together to a separation distance of 1.5 Å. The system is subsequently thermalized at a temperature of 300 K using the Langevin dynamics approach. To ensure a coherent interface, the parameters of Si potential are adjusted so that the Si(111) and $Si_3N_4(0001)$ surfaces match exactly. Once the interface is formed, we gradually revert to the original model to introduce the lattice mismatch in a continuous fashion. Finally, the system is again thermalized at 300 K. Two sets of nanopixels were simulated; Fig. 1(a) shows a schematic diagram. The 3.7×10^6 atom square nanopixel consists of a 256 Å $\times$ 257 Å $\times$ 83 Å crystalline Si_3N_4 film placed on a 10-Å-thick Si mesa on top of a 512 Å $\times$ 513 Å $\times$ 257 Å Si substrate. For the ten-million-atom simulation the system consists of a 540 Å $\times$ 327 Å $\times$ 83 Å crystalline Si_3N_4 film placed on a 10-Å-thick Si mesa on top of a 1077 Å $\times$ 653 Å $\times$ 257 Å Si substrate. Periodic boundary conditions are used in the *XY* plane and the bottom layer of Si atoms in the substrate is fixed to the lattice constant of bulk Si.

Figure 1(b) shows the interface structure observed in the nanopixel. The atoms in the top layer of Si atoms in silicon are bonded with N atoms in silicon nitride and a coherent interface is formed. The Si/Si_3N_4 interface induces significant deformation in Si seen in the bond-length distributions in the Si mesa computed at $T = 0$ K. The Si-Si bond between first and second Si layers [Fig. 1(c)] has a broad distribution of lengths consisting of three main peaks. Figure 1(d) corresponds to bonds between second and third layers, where we observe two peaks. The bond-length distribution in the bulk is also broadened due to strain induced by the interface. The form of the bond-length distribution near the interface is due to different environments faced by silicon atoms at the interface with Si_3N_4.

The nanopixel with an amorphous Si_3N_4 film [Fig. 2(a)] is prepared as follows. First, a bulk amorphous Si_3N_4 system is produced by quenching a molten system with periodic boundary conditions. During this procedure, a layer of Si and N atoms is kept fixed at the crystalline Si_3N_4 atomic positions to facilitate subsequent bonding with the silicon system. The periodic boundary conditions are then removed and an amorphous Si_3N_4 film of appropriate dimensions is cut out of the bulk system. The Si_3N_4 film is placed at a distance of 6 Å from the silicon mesa with the fixed layer of atoms facing the Si surface, and the same preparation procedure is followed as in the case of crystalline Si_3N_4. Once the interface is established, the fixed layer of Si_3N_4 is released and the system is quenched and thermalized at 300 K. As a result, the interface becomes disordered, as shown in Fig. 2(b). The peak structure in the interface bond-length distributions disappears

[Figs. 2(c), 2(d), and 2(e)] and the distributions are broadened compared to those for the crystalline Si_3N_4 system (see Fig. 1).

Figure 3 shows the color-coded local pressure distribution, $p = (\sigma_{xx} + \sigma_{yy} + \sigma_{zz})/3$, for the ten-million-atom nanopixel covered with crystalline (a) and amorphous (b) silicon nitride, respectively. Since $Si_3N_4(0001)$ is 1.1% larger than Si(111), the mismatch results in compressive stress for silicon nitride at the interface and tensile stress for silicon [see Fig. 3(a)]. The largest stress values of about -2 GPa are seen just below the interface. Furthermore, the lattice mismatch gives rise to a parabolic stress well which goes deep into the substrate, the region where the device operates. For the case of amorphous silicon nitride [see Fig. 3(b)] we observe large stress fluctuations due to nonuniformity of local density in the silicon nitride layer. The hydrostatic stress variation along the Z axis through the center in the two nanopixels is plotted (yellow circles) in Fig. 4. Owing to the stress fluctuations inherent in the amorphous state at the interface, the tensile stress in Si at the interface is much smaller in the case of amorphous Si_3N_4.

To investigate the effect of amorphous silicon nitride on the nature of stresses in the XY plane, we have computed stress distributions for three slices parallel to the interface for 25 nm $\times$ 25 nm and 54 nm $\times$ 33 nm mesas. In the 54 nm $\times$ 33 nm mesa with crystalline silicon nitride, Fig. 5(a) shows the stress distribution in silicon nitride parallel to the interface—compressive stresses determined by the larger lattice constant compared to silicon. The stress in the silicon just below the interface [Fig. 5(b)] is highly tensile in the center and decreases towards the edges. The values for the stress in the silicon substrate [Fig. 5(c)] decrease considerably due to the spatial distance from its source, the interface with silicon nitride. A shadow of the edges and corners of the mesa are also visible deep in the substrate.

The symmetry of the stress pattern and the effect of the mesa shape—square to rectangular—can be understood from Figs. 5(d)–5(i). The first three figures, 5(d)–5(f), show stresses for three horizontal slices for the 25 nm square mesa. Threefold symmetry of Si(111) catalyzes the ordering of stress fluctuations at the interface resulting in three tensile stress domains seen in silicon mesa below the interface and in the substrate. Figures 5(g)–5(i) show stress patterns in the same three horizontal layers for the 54 nm $\times$ 33 nm rectangular mesa. The aspect ratio for 54 nm $\times$ 33 nm mesa is less than 2 so that two threefold patterns like the ones shown in Figs. 5(d)–5(f) cannot be comfortably accommodated. The stress patterns in Figs. 5(g)–5(i) are a result of squeezing together two triangular patterns, resulting in an approximate Y-like shape with the longer leg of the Y being in the direction of the longer length of the mesa.

State-of-the-art parallel computers make is possible to perform atomistic simulations for structures of submicron size [16–18]. In our study of atomistic stresses of silicon

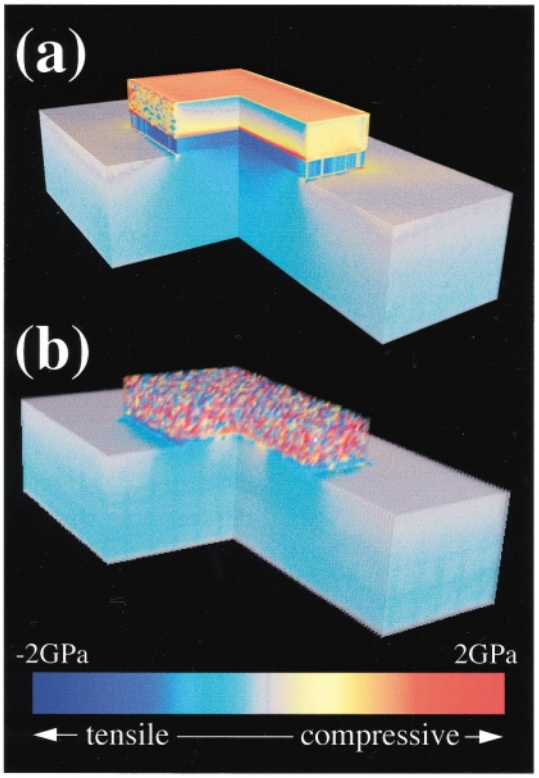

FIG. 3 (color). Hydrostatic stress distribution in nanopixels: (a) top layer crystalline Si_3N_4, and (b) top layer amorphous Si_3N_4 films. The value of the stress is color coded according to the color bar at the bottom (compressive stress is assumed positive).

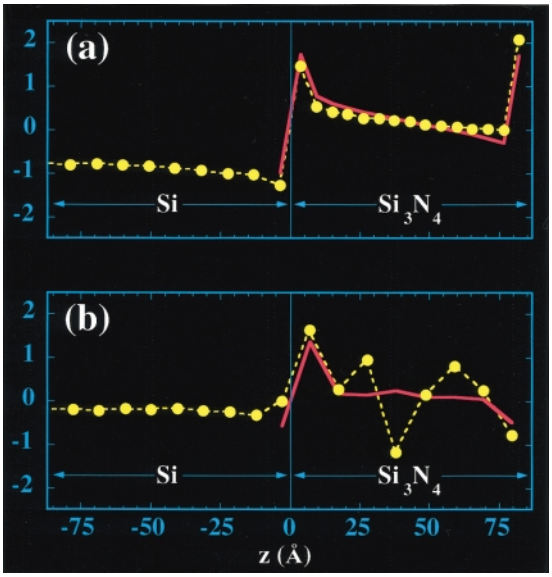

FIG. 4 (color). Hydrostatic stress variation along the z axis through the center of the nanopixel: (a) $Si(111)/Si_3N_4(0001)$ and (b) $Si(111)/a\text{-}Si_3N_4$ systems. The stress averaged over XY slices is shown with a solid magenta line.

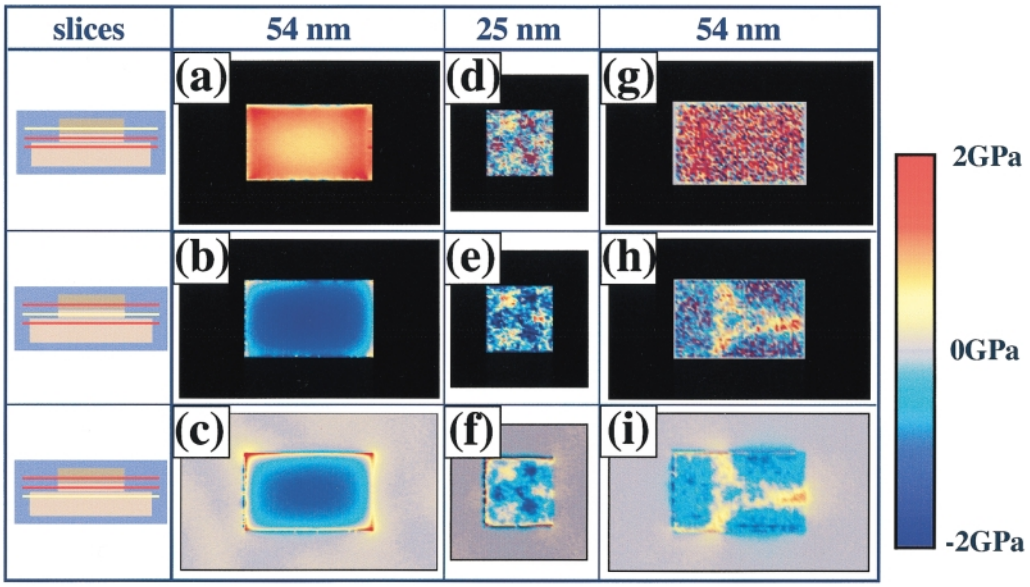

FIG. 5 (color). Horizontal cross sections of the stress distribution in nanopixels covered with crystalline and amorphous Si_3N_4 for two different system sizes. The slices are taken through (a) Si_3N_4 above the interface, (b) Si mesa below the interface, and (c) Si substrate for the 54 nm $\times$ 33 nm mesa covered with crystalline Si_3N_4; (d), (e), and (f) are the corresponding slices for the case of the 25 nm square mesa covered with amorphous Si_3N_4; and (g), (h), and (i) are the slices for the case of the 54 nm $\times$ 33 nm mesa covered with amorphous Si_3N_4.

nanopixels covered with a crystalline or amorphous silicon nitride layer we have found several sources of stress concentrations. The lattice mismatch of 1.1% between silicon nitride and silicon yields to high compressive stresses in silicon nitride at the interface and high tensile stresses in silicon at the interface. The parabolic tensile stress well in silicon goes deep into the substrate. Amorphous silicon nitride shows high stress fluctuations which align at the interface with Si(111) to form tensile stress domains in the silicon below it. For the 3.7×10^6 atom system with a 25 nm square mesa, stress domains with triangular symmetry are observed in silicon below the interface reflecting the symmetry of Si(111). For the ten-million-atom rectangular mesa of 54 nm $\times$ 33 nm size, two triangular stress patterns get squeezed together, forming a Y-shaped compressive stress wall with the longer leg of the Y being in the direction of the longer length of the nanopixel. The elongated Y-like tensile stress domains are about 300 Å in size. The domain size is comparable to the dimensions of the nanopixel, which would result in uneven dopant distribution and significantly effect the performance of electronic devices. Pixel sizes on the order or less than 50 nm are currently being considered by industry and government agencies.

This work was supported by the Austrian FWF, DOE, NSF, AFOSR, USC-LSU MURI, and ARO. Ten-million-atom simulations were carried out on the 256-processor HP Exemplar at Caltech. Access to the Exemplar was provided by the National Partnership for Advanced Computational Infrastructure (NPACI) through a cooperative agreement with the National Science Foundation.

[1] A. Y. Liu and M. L. Cohen, Phys. Rev. B **41**, 10 727 (1990).
[2] A. Reyes-Serrato *et al.*, Phys. Rev. B **52**, 6293 (1995).
[3] G. L. Zhao and M. E. Bachlechner, Europhys. Lett. **37**, 287 (1997); Phys. Rev. B **58**, 1887 (1998).
[4] M. Z. Bazant and E. Kaxiras, Phys. Rev. Lett. **77**, 1 (1996).
[5] F. S. Khan and J. Q. Broughton, Phys. Rev. B **39**, 3688 (1989).
[6] D. K. Ferry and S. M. Goodnick, *Transport in Nanostructures* (Cambridge University Press, Cambridge, 1997).
[7] F. Liu *et al.*, Chem. Rev. **97**, 1045 (1997).
[8] W. Yu and A. Madhukar, Phys. Rev. Lett. **79**, 905 (1997); **79**, 4939(E) (1997).
[9] S. C. Jain *et al.*, J. Appl. Phys. **78**, 1630 (1995).
[10] M. E. Bachlechner *et al.*, Mater. Res. Soc. Symp. Proc. **446**, 157 (1997).
[11] F. H. Stillinger and T. A. Weber, Phys. Rev. B **31**, 5262 (1985).
[12] P. Vashishta *et al.*, in *Amorphous Insulators and Semiconductors*, edited by M. F. Thorpe and M. I. Mitkova, NATO ASI, Vol. 23 (Kluwer, Dordrecht, 1997).
[13] P. Vashishta *et al.*, Phys. Rev. Lett. **75**, 858 (1995); A. Nakano *et al.*, Phys. Rev. Lett. **75**, 3138–3141 (1995).
[14] A. Stesmans and G. V. Gorp, Phys. Rev. B **52**, 8904–8920 (1995); E. Bauer *et al.*, Phys. Rev. B **51**, 17 891 (1995).
[15] V. S. Kaushik *et al.*, Appl. Phys. Lett. **52**, 1782–1784 (1988).
[16] F. F. Abraham, Phys. Rev. Lett. **77**, 869 (1996).
[17] R. L. B. Selinger *et al.*, *Fracture—Instability, Dynamics, Scaling, and Ductile/Brittle Behavior* (MRS, Pittsburgh, 1996).
[18] S. J. Zhou and B. L. Holian, Phys. Rev. Lett. **78**, 479 (1997).